

Controlled vapor growth of 2D magnetic Cr_2Se_3 and its magnetic proximity effect in heterostructures

Danliang Zhang(张丹亮), Chen Yi(易琛), Cuihuang Ge(葛翠环), Weining Shu(舒维宁), Bo Li(黎博), Xidong Duan(段曦东), Anlian Pan(潘安练), and Xiao Wang(王笑)

Citation: Chin. Phys. B, 2021, 30 (**9**): 097601. DOI: 10.1088/1674-1056/ac0cd9
Journal homepage: http://cpb.iphy.ac.cn; http://iopscience.iop.org/cpb

What follows is a list of articles you may be interested in

Effect of interface magnetization depinning on the frequency shift of ferromagnetic and spin wave resonance in YIG/GGG films

Fanqing Lin(林凡庆), Shouheng Zhang(张守珩), Guoxia Zhao(赵国霞), Hongfei Li(李洪飞), Weihua Zong(宗卫华), Shandong Li(李山东)

Chin. Phys. B, 2020, 29 (**6**): 067601. DOI: 10.1088/1674-1056/ab8dac

Large tunable FMR frequency shift by magnetoelectric coupling in oblique-sputtered $Fe_{52.5}Co_{22.5}B_{25.0}$/PZN-PT multiferroic heterostructure

Zhi-Peng Shi(时志鹏), Xiao-Min Liu(刘晓敏), Shan-Dong Li(李山东)

Chin. Phys. B, 2017, 26 (**9**): 097601. DOI: 10.1088/1674-1056/26/9/097601

Magnetic transition behavior of perovskite manganites $Nd_{0.5}Sr_{0.3}Ca_{0.2}MnO_3$ polycrystalline

Ru Xing(邢茹), Su-Lei Wan(万素磊), Wen-Qing Wang(王文清), Lin Zheng(郑琳), Xiang Jin(金香), Min Zhou(周敏), Yi Lu(鲁毅), Jian-Jun Zhao(赵建军)

Chin. Phys. B, 2016, 25 (**4**): 047601. DOI: 10.1088/1674-1056/25/4/047601

Microwave reflection properties of planar anisotropy $Fe_{50}Ni_{50}$ powder/paraffin composites

Wei Jian-Qiang,Zhang Zhao-Qi,Han Rui,Wang Tao,Li Fa-Shen

Chin. Phys. B, 2012, 21 (**3**): 037601. DOI: 10.1088/1674-1056/21/3/037601

SPECIAL TOPIC – Two-dimensional magnetic materials and devices

Controlled vapor growth of 2D magnetic Cr_2Se_3 and its magnetic proximity effect in heterostructures*

Danliang Zhang(张丹亮)[1,†], Chen Yi(易琛)[2,†], Cuihuan Ge(葛翠环)[1], Weining Shu(舒维宁)[1], Bo Li(黎博)[1], Xidong Duan(段曦东)[3], Anlian Pan(潘安练)[2,‡], and Xiao Wang(王笑)[1,§]

[1] *School of Physics and Electronics, Hunan University, Changsha* 410082, *China*

[2] *Key Laboratory for Micro-Nano Physics and Technology of Hunan Province, College of Materials Science and Engineering, Hunan University, Changsha* 410082, *China*

[3] *Hunan Key Laboratory of Two-Dimensional Materials and State Key Laboratory for Chemo/Biosensing and Chemometrics, College of Chemistry and Chemical Engineering, Hunan University, Changsha* 410082, *China*

(Received 13 April 2021; revised manuscript received 28 May 2021; accepted manuscript online 21 June 2021)

Two-dimensional (2D) magnetic materials have aroused tremendous interest due to the 2D confinement of magnetism and potential applications in spintronic and valleytronic devices. However, most of the currently 2D magnetic materials are achieved by the exfoliation from their bulks, of which the thickness and domain size are difficult to control, limiting the practical device applications. Here, we demonstrate the realization of thickness-tunable rhombohedral Cr_2Se_3 nanosheets on different substrates via the chemical vapor deposition route. The magnetic transition temperature at about 75 K is observed. Furthermore, van der Waals heterostructures consisting of Cr_2Se_3 nanosheets and monolayer WS_2 are constructed. We observe the magnetic proximity effect in the heterostructures, which manifests the manipulation of the valley polarization in monolayer WS_2. Our work contributes to the vapor growth and applications of 2D magnetic materials.

Keywords: Cr_2Se_3, magnetic proximity effect, heterostructures

PACS: 76.50.+g, 75.70.Cn, 42.25.Ja **DOI:** 10.1088/1674-1056/ac0cd9

1. Introduction

The emerging two-dimensional (2D) magnetic materials provide an ideal system for both basic physics and spintronic applications due to their unique 2D-limited magnetism and spin states on the nanomater scale.[1–3] Combining 2D magnetic and non-magnetic (semiconductor) materials can form a new type of Van der Waals (vdW) heterostructures, in which the so called magnetic proximity effect could play an import role. The effect is highly sensitive to the interfacial electronic properties and has opened up new opportunities to manipulate spintronics, superconductivity, excitonic and topological phenomena.[4] The manipulation of spintronics and valleytronics in 2D vdW heterostructures using the magnetic proximity effect has been demonstrated, manifesting an enhanced valley Zeeman splitting and/or modifications of the valley polarization.[4–10]

The controllable realization of high-quality 2D magnetic materials is crucial for the investigation of the magnetic proximity effect and also potential device applications. 2D magnetic materials, such as Fe_3GeTe_2, $Cr_2Ge_2Te_6$, CrI_3 atomic layers, are mainly obtained via the mechanical exfoliation from their bulk counterparts,[11–14] which has difficulties in controlling the thickness, domain size and the obtained layers are relatively unstable in air. Recently, the wafer-scale thin films of Fe_3GeTe_2 were obtained via a molecular beam epitaxy (MBE) method, which could promote the realization of practical devices.[15] In contrast, 2D non-layered materials have strong chemical bonds instead of Van der Waals interaction among the layers, therefore, they are hard to obtain via the mechanical exfoliation method. Chemical vapor deposition (CVD) route has been utilized to prepare air-stable and large size nonlayered magnetic materials such as Cr_2S_3, CrSe, and Cr_2Te_3, which exhibit excellent optical, electrical, and magnetic properties.[16–20] Such materials with different stoichiometry can be obtained by controlling the growth conditions, such as deposition temperature, carrier gas, and source ratio.[21–23] Very recently, bulk chromium selenium (Cr_2Se_3) was obtained experimentally and the crystal structure and magnetic properties were investigated as well.[24] However, ultrathin 2D Cr_2Se_3 nonlayered magnetic materials and the related photophysics have not yet been explored. Moreover, Cr_2Se_3-based vdW heterostructures of related magnetic applications in spintronics and valleytronics are desirable to be explored.

*Project supported by the National Natural Science Foundation of China (Grant Nos. 52022029, 91850116, 51772084, 62090035, and U19A2090), Hunan Provincial Natural Science Foundation of China (Grant Nos. 2018RS3051 and 2018WK4004), and the Key Program of the Hunan Provincial Science and Technology Department (Grant No. 2019XK2001).

†These authors contributed equally.

‡Corresponding author. E-mail: anlian.pan@hnu.edu.cn

§Corresponding author. E-mail: xiao_wang@hnu.edu.cn

© 2021 Chinese Physical Society and IOP Publishing Ltd

In this work, we realize the synthesis of thickness-tunable and air-stable rhombohedral single-crystal Cr_2Se_3 via the CVD method. Single-unit-cell thick ($\approx$ 1.8 nm) Cr_2Se_3 nanosheets and thicker nanosheets with a lateral length of 120 μm are successfully obtained. By constructing vdW magnetic heterostructures with ultrathin 2D Cr_2Se_3 nanosheets and monolayer WS_2, we investigate the magnetic proximity effect in the heterostructures and the related manipulation of spin and valley pseudospin in monolayer WS_2. Our findings contribute to the controlled growth of new 2D magnetic materials and the understanding and utilization of magnetic proximity effect.

2. Experimental details

The growth of Cr_2Se_3 nanosheets was carried out in a single-temperature-zone tube furnace by a CVD route (Fig. 1(a)). A ceramic boat with selenium (Se) powder (99.9%, Alfa) was placed in the upstream area of the tube furnace. The mixed powders of chromium (Cr; 99%, Alfa) and sodium chloride (NaCl; 99.99%, Alfa) with a weight ratio of 10:1 were loaded in the other ceramic boat, and a fresh and clean growth substrate (fluorophlogopite ($[KMg_3(AlSi_3O_{10})F_2]$) mica, 300 nm-SiO_2/Si or glassy silica substrate) was placed directly above it. The ceramic boat was placed in the central heating zone of the tube furnace. Notably, the NaCl powder was used to lower the melting point of the Cr powder (melting point is 1857 °C) and the energy barrier as well as to increase the reaction rate.[25,26] The temperature of the tube furnace was increased from room temperature to 820–900 °C within 25–30 min with the Ar flow rate of 60 sccm, and the furnace temperature was maintained for 3–5 min for sample growth. Finally, the Cr_2Se_3 nanosheets with different thicknesses were obtained. The results suggest that the fluorophlogopite mica substrate with chemically inert surface and atomic flat is conducive to the epitaxial growth of thinner Cr_2Se_3 samples.[27]

For constructing the heterostructure, the monolayer WS_2 exfoliated from their bulks was transferred to the thin Cr_2Se_3 nanosheet surface by the PDMS-assisted dry transfer method. To enhance the coupling of the heterostructures interface, the WS_2/Cr_2Se_3 heterostructure sample was placed in a vacuum annealing furnace set at 180 °C for 8 hours.

To further understand the morphology and atomic structure, the CVD-synthesized Cr_2Se_3 nanosheets were characterized via optical microscope (Axio Scope A1, Zeiss), atomic force microscope (AFM, Multimode 8, Bruker), x-ray diffraction (XRD, MiniFlex 600, Rikaga), x-ray photoemission spectroscopy (XPS, 250Xi, ESCALAB), scanning electron microscope (SEM, SIGMA HD, Zeiss), and transmission electron microscopy (TEM, Tecnai G2-20, FEI). High-resolution TEM (HRTEM) and selected area electron diffraction (SAED) measurements were also performed to identify the atomic structure and crystallinity of the triangle-shaped Cr_2Se_3 nanosheets. The physical property measurement system (PPMS, DynaCool 9, Quantum Design) was used to measure the magnetic properties of the CVD grown samples.

Raman spectroscopy of the Cr_2Se_3 nanosheets was performed by a confocal optical microscope (WITec, alpha-300) under the excitation of a continuous wave laser at 532 nm. Circular polarization-resolved photoluminescence (PL) spectroscopy was recorded with a 488 nm laser, and the optical path and experimental details are the same as reported in our previous studies.[28,29] It is worth noting that in this study we always collected the PL emission with the same circular polarization as that of the excitation. We define the PL degree of circular polarization (ρ) as $\rho_{PL} = (I_{\sigma+/\sigma+} - I_{\sigma-/\sigma-})/(I_{\sigma+/\sigma+} + I_{\sigma-/\sigma-})$, where $I_{\sigma+/\sigma+}$ ($I_{\sigma-/\sigma-}$) represents the PL intensity under both $\sigma+$ ($\sigma-$) excitation and $\sigma+$ ($\sigma-$) detection.

3. Results and discussion

Based on the described growth method, we successfully prepared thickness controllable 2D Cr_2Se_3 nanosheets. The non-layered Cr_2Se_3 single crystal displays the single-unit-cell with abc stacking sequence and the thickness of about 1.8 nm (Fig. 1(b)). The top and side views of the Cr_2Se_3 crystal structure are shown in supporting information Fig. S1. Figure 1(c) displays the AFM image of the CVD-synthesized Cr_2Se_3 nanosheet obtained from a mica substrate showing a smooth surface with a thickness of about 1.8 nm, which corresponds to the one-unit-cell thickness of Cr_2Se_3. To control the thickness of grown Cr_2Se_3, we precisely controlled the heating temperature while keeping other growth parameters (such as growth time, gas flow) constant during the CVD growth process. Figure 1(d) shows typical optical images of Cr_2Se_3 grown on mica substrate at different growth temperatures. It is clear that the Cr_2Se_3 nanosheets evidently grow thicker and larger with increasing the temperature. The corresponding thickness varied from $\sim$1.8 nm to tens of nanometers confirmed by the AFM measurement, when the temperature was increases from 820 °C to 900 °C. We also tested the stability of the CVD-synthesized Cr_2Se_3. According to the AFM image, we observed no obvious changes from the nanosheet after 283 days (supporting information Fig. S2). Figure 1(e) shows the optical image of a large area thicker non-layered Cr_2Se_3 (approximately 10 nm) grown on mica. Hexagon and triangle-shaped Cr_2Se_3 nanosheets distribute throughout the substrate. The inset of Fig. 1(e) shows the Cr_2Se_3 nanosheet with a lateral length of 120 μm. In order to explore the influence of the substrate on growth, the 300 nm-SiO_2/Si and glassy silica substrates were used as well. The Cr_2Se_3 tends to grow triangle-shaped samples on the 300 nm-SiO_2/Si and glassy silica substrates (Figs. 1(f) and 1(g)). To explore the crystal vibrational properties, Raman spectroscopy was used

to measure the Cr_2Se_3 nanosheets. The Raman spectra of the as-grown Cr_2Se_3 nanosheets on the mica substrate with different thicknesses varying from 6 nm to 26 nm were collected (Fig. 1(h)). The Raman mode at 253 cm^{-1} redshifts as the thickness increases, showing a clear thickness dependence. The two characteristic Raman peak mappings extracted from the integrated intensities of 145 cm^{-1} and 253 cm^{-1} indicate uniform crystallinity under 532 nm laser excitation (supporting information Figs. S3a and S3b).

The XRD was used to investigate the crystal structure of the CVD-synthesized Cr_2Se_3 nanosheets on SiO_2/Si substrate (Fig. 2(a)). The observed four prominent diffraction peaks well match the standard PDF card (PDF#89-2068) from the rhombohedral Cr_2Se_3 of [001] crystal plane. Based on the XRD data, the crystal structure geometry of Cr_2Se_3 belongs to the space group $R\bar{3}$ with the lattice constants of $a = b = 6.254$ Å and $c = 17.382$ Å, which is consistent with the previous studies.[24,30] To determine the chemical states and elemental composition, the CVD-grown sample was measured by XPS (Figs. 2(b) and 2(c)). The two doublet peaks in the Cr 2p spectra correspond to the chemical states of Cr $2p_{1/2}$ and $2p_{3/2}$, with the first pair locating at 584.0 eV and 574.5 eV, while the second pair appearing at 586.2 eV and 576.8 eV attributed to the satellite peaks. In the Se 3d spectra (Fig. 2(c)), the peaks at around 55.3 eV and 54.2 eV represent the Se $3d_{3/2}$ and $3d_{5/2}$, respectively. For the transmission electron microscopy characterization, the as-grown samples on the SiO_2/Si substrate were transferred to the carbon-supported copper grid via the PMMA-assisted transfer route.[31] Figure 2(d) shows the HRTEM image of Cr_2Se_3 with a clear hexagonal atomic arrangement, extracted from which the (110) crystal plane spacing is about 0.31 nm. Figure 2(e) shows the corresponding SAED pattern with the six equivalent diffraction spots from the (110) lattice planes. The existence of one set of spots in the SAED pattern demonstrates the single crystal nature of the Cr_2Se_3. The inset of Fig. 2(e) shows the low-magnification TEM image of the Cr_2Se_3 nanosheet. The elemental composition of the synthesized Cr_2Se_3 crystals can be further analyzed by energy-dispersive spectroscopy (EDS) spectroscopy. The Cr:Se atomic ratio is calculated to be 38.6:61.4, close to 2:3 through the computation of peak areas, confirming the formation of stoichiometric hexagonal phase Cr_2Se_3 (Fig. 2(f)).[30,32] Figure 2(g) shows the representative SEM image of the Cr_2Se_3 nanosheet on mica substrate. The Cr_2Se_3 nanosheet is smooth and clean across the whole sample region. The corresponding SEM elemental mappings are shown in Figs. 2(h) and 2(i). Based on the SEM results, we can confirm that the synthesized Cr_2Se_3 nanosheets consist of uniform distributed Cr and Se elements. The atomic ratio

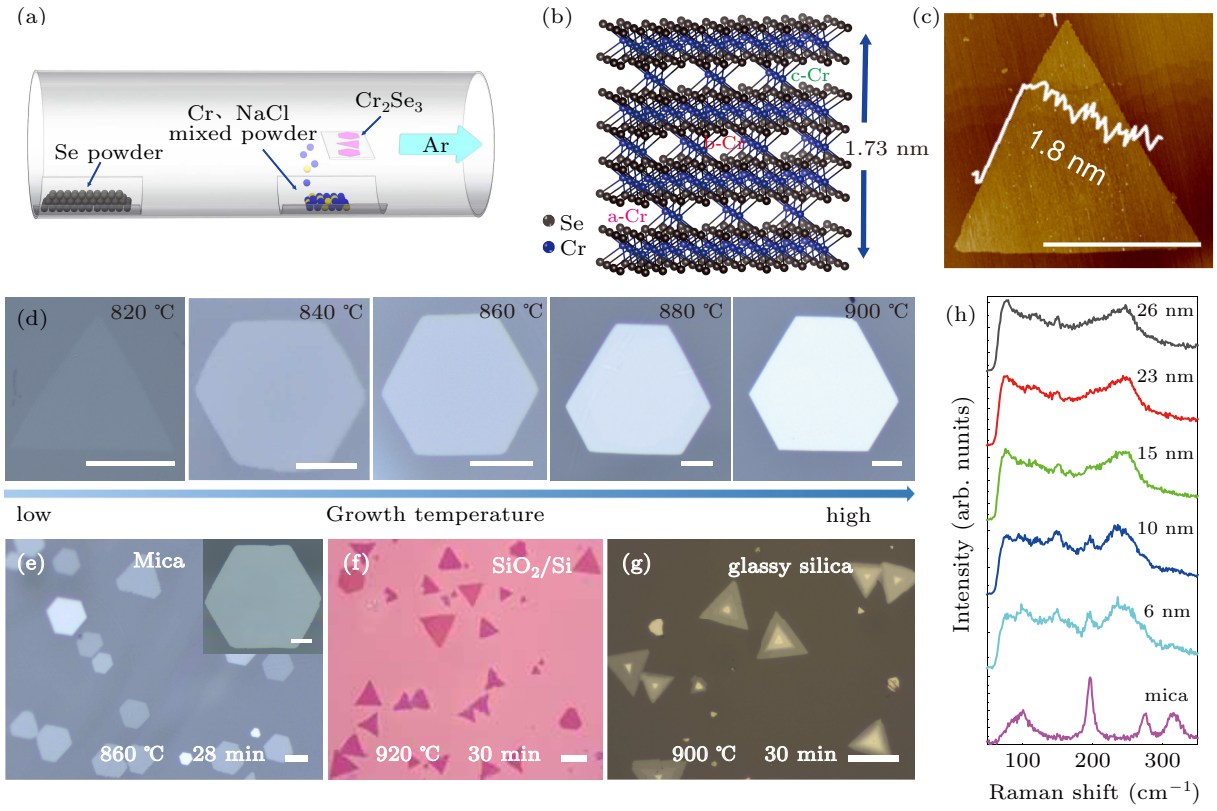


Fig. 1. (a) Schematic illustration of the CVD growth process of Cr_2Se_3 nanosheets, gray: Se powder, blue: Cr, yellow: NaCl powder. (b) Structural model of the Cr_2Se_3 crystal. (c) AFM image of the triangle-shaped Cr_2Se_3 with the thickness of 1.8 nm (one-unit-cell). (d) Growth-temperature dependent bright-field optical images of as-grown Cr_2Se_3 nanosheets under growth conditions of 820–900 °C over 25 min. (e)–(g) Typical bright-field optical images of Cr_2Se_3 nanosheets on (e) mica, (f) SiO_2/Si, and (g) glassy silica substrates. The inset of (e) shows a Cr_2Se_3 nanosheet with a lateral length of 120 μm. (h) Raman spectra of the Cr_2Se_3 nanosheets with different thicknesses. All scale bar: 20 μm..

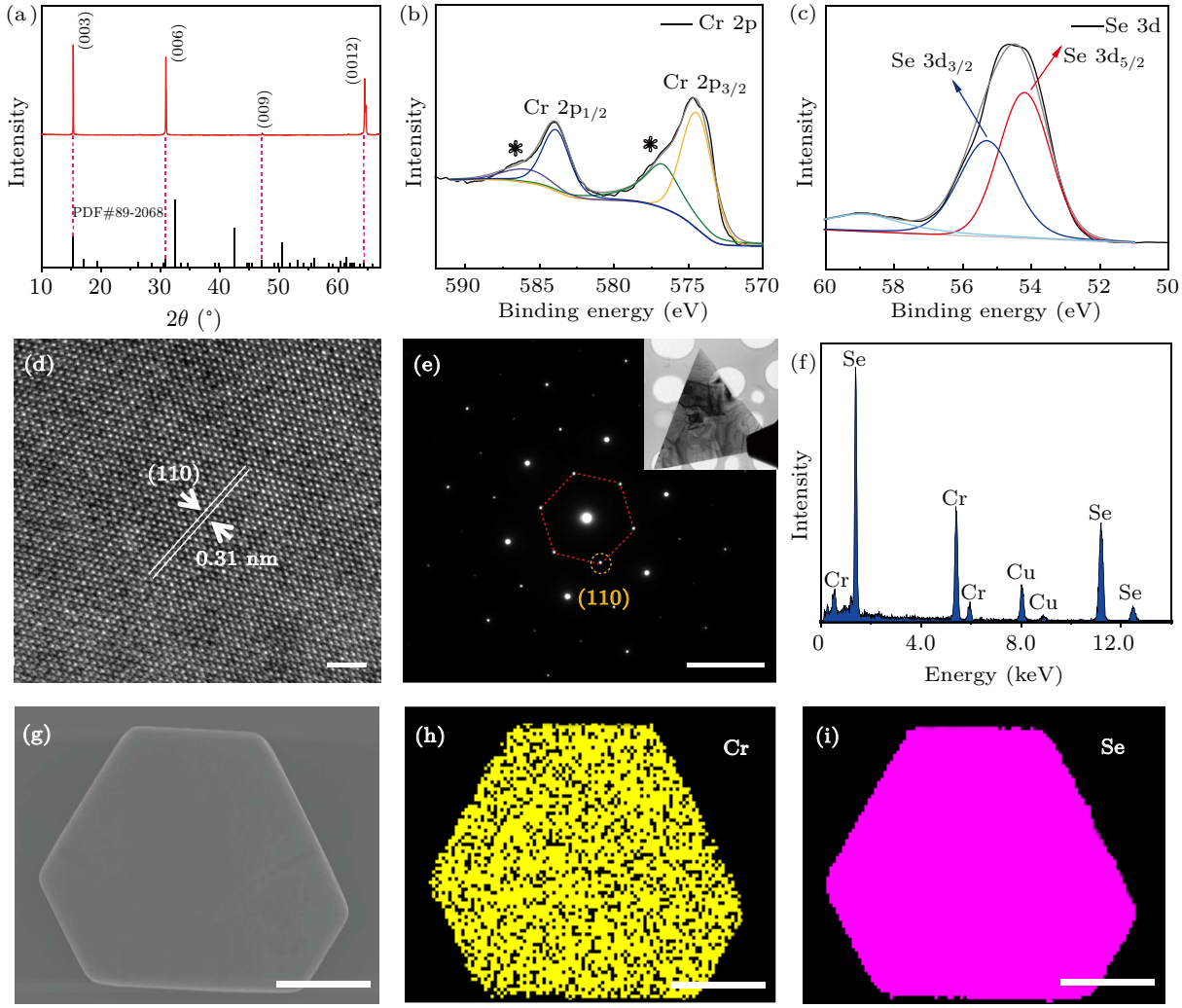


Fig. 2. (a) XRD spectra of thicker Cr_2Se_3 nanosheets. (b), (c) XPS spectra from Cr 2p peaks and Se 3d peaks of the Cr_2Se_3 nanosheets. (d) HRTEM image of the Cr_2Se_3 nanosheet; scale bar: 2 μm. (e) The corresponding SAED patterns of the Cr_2Se_3 nanosheet; scale bar: 5 nm^{-1}. The low-magnification TEM image of the Cr_2Se_3 nanosheet is shown in the inset. (f) EDX spectrum of the Cr_2Se_3 nanosheet. (g) SEM image of a Cr_2Se_3 nanosheet and its corresponding SEM elemental mappings of Cr (h) and Se atoms (i). Scale bar: 3.5 μm.

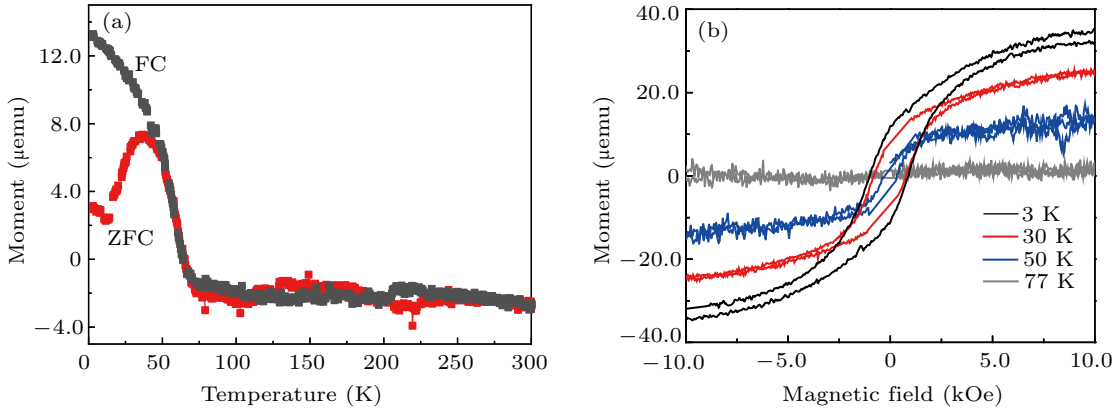


Fig. 3. (a) The temperature dependent magnetization of Cr_2Se_3 nanosheets on SiO_2/Si substrate under a parallel magnetic field of 1000 Oe. The ZFC process is represented by the red curve; the FC process is represented by the gray curve. (b) Magnetic hysteresis loop from the Cr_2Se_3 nanosheets at different temperatures with a parallel magnetic field.

of Cr and Se elements is 38.76:61.24, similar as the data from EDS, which further confirms the composition information of the sample. Similar SEM results were obtained from the samples grown on glassy silica and SiO_2/Si substrates (supporting information Fig. S4). There is no obvious difference in the structure and properties of the samples grown on these three substrates. The high-quality Cr_2Se_3 sample enables it as an ideal candidate for further research and applications, especially for designing novel spintronics and valleytronics with simpler structures.

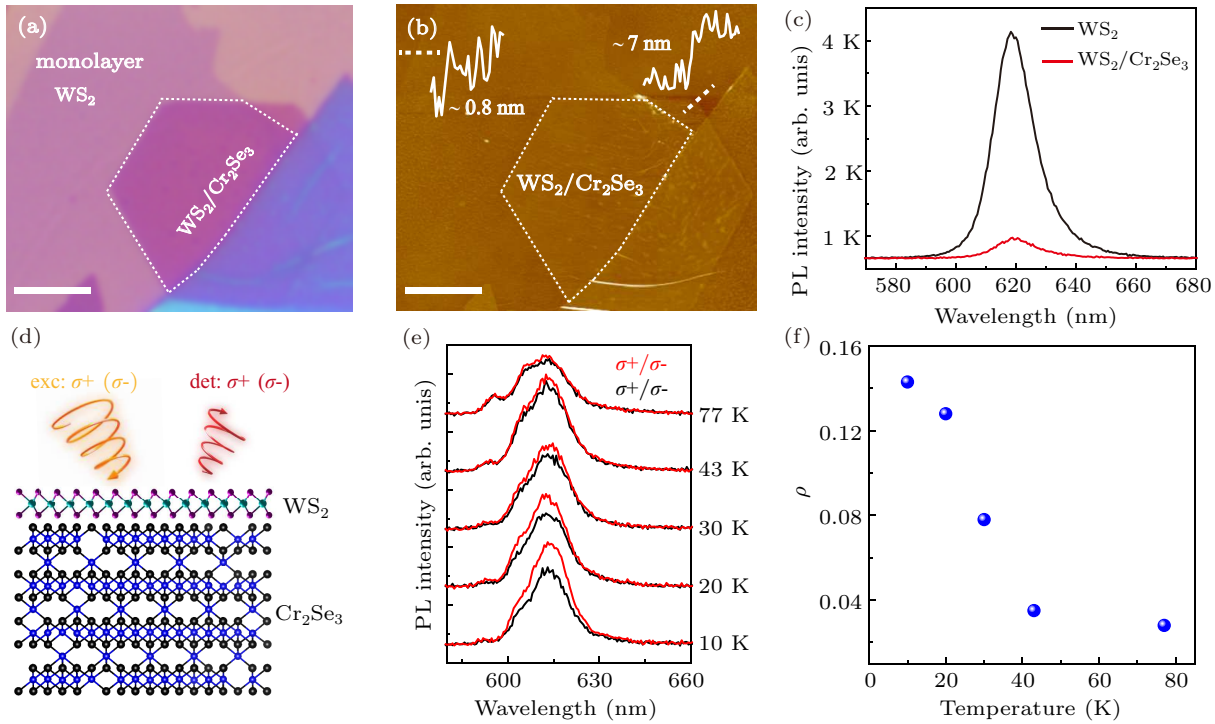


Fig. 4. (a) Bright-field optical image of the WS_2/Cr_2Se_3 heterostructure on SiO_2/Si substrate. (b) The corresponding AFM image with height profile of the sample in (a). (c) Typical PL spectra from the WS_2/Cr_2Se_3 heterostructure region and bare monolayer WS_2, respectively. (d) Schematic illustration of the polarization experiments for the WS_2/Cr_2Se_3 heterostructure. Only the PL emission with the same circular polarization as the excitation was collected. (e) Circularly polarized PL spectra of the WS_2/Cr_2Se_3 heterostructure at different temperatures. (f) The temperature-dependent ρ of the monolayer WS_2 PL from the heterostructure.

To identify the magnetic properties of the CVD-synthesized Cr_2Se_3 samples, almost film-forming Cr_2Se_3 samples with a thickness up to micron on the SiO_2/Si substrate were investigated by a physical property measurement system. Figure 3(a) shows the temperature-dependent magnetic moments under the parallel magnetic field of 1000 Oe, which shows the obvious magnetic properties of the CVD-synthesized Cr_2Se_3. The zero-field-cooled (ZFC) and field-cooled (FC) curves show the magnetic transition temperature at about 75 K and indicate a net magnetic moment below the magnetic transition temperature, which is consistent with the previous reports.[24,33] Furthermore, the temperature dependent magnetic hysteresis loops under the parallel magnetic field scanning within ± 1 T are shown in Fig. 3(b). The results show that there is obvious magnetic hysteresis at the temperature range from 3 K to 77 K. According to the previous studies, the out-of-plane hysteresis of Cr_2Se_3 crystals is much stronger than that of in-plane.[24] The obvious magnetic properties of the CVD-grown Cr_2Se_3 nanosheets provide a good opportunity for the manipulation of spin/valley physics.

To further investigate the magnetic proximity effect of the CVD-grown Cr_2Se_3 nanosheets, the van der Waals heterostructures consisting of a bottom ultrathin CVD-grown Cr_2Se_3 nanosheet and a top mechanically exfoliated monolayer WS_2 were fabricated with the dry transfer method, which was operated under ambient condition. There is no further encapsulation for the heterostructures. Monolayer WS_2 with rich pseudospin and valley degrees of freedom is a typical non-magnetic semiconductor, which can be manipulated using circularly polarized light.[28,29,34] The optical microscope image of the WS_2/Cr_2Se_3 heterostructure is shown in Fig. 4(a), of which the heterostructure region is framed by white dashed lines. The corresponding AFM image (Fig. 4(b)) shows the top WS_2 and the bottom Cr_2Se_3 with the thicknesses of about 0.8 nm and 7 nm, respectively. The relative thin layers could enable the magnetic proximity effect in the WS_2/Cr_2Se_3 heterostructures. Under linearly polarized laser excitation, typical PL spectra collected from the heterostructure region and that from the bare monolayer WS_2 are compared in Fig. 4(c). The PL intensity of WS_2 from the WS_2/Cr_2Se_3 heterostructure region is significantly quenched compared to that of pure monolayer WS_2, which is attributed to the transfer of carriers from the top monolayer WS_2 to the bottom Cr_2Se_3. The circular polarization-resolved PL measurements from the WS_2/Cr_2Se_3 heterostructure were further investigated, without introducing any additional magnetic dopants or field. Figure 4(d) schematically illustrates the circularly polarized light excitation and PL emission of the WS_2 in a WS_2/Cr_2Se_3 heterostructure. Theoretically, the $\pm K$ valley is degenerate and the PL degree of circular polarization $\rho = (I_{\sigma+/\sigma+} - I_{\sigma-/\sigma-})/(I_{\sigma+/\sigma+} + I_{\sigma-/\sigma-})$ is zero without external magnetic field due to the time reversal symmetry.[35] However, since the monolayer WS_2 is adjacent to the magnetic Cr_2Se_3, ρ is expected to have a larger value, and its sign should be directly related to the bottom Cr_2Se_3 magnetization direction.[8] Figure 4(e) displays the temperature-dependent circularly polarized PL spectra of

the WS_2/Cr_2Se_3 heterostructures. The valley degeneracy and time reversal symmetry of monolayer WS_2 are broken due to the adjacent 2D magnetic Cr_2Se_3.[4] The PL intensity under the $\sigma+$ excitation and $\sigma+$ detection ($\sigma+/\sigma+$, red curve) is always stronger than that of the $\sigma-/\sigma-$ configuration (black curve), indicating the non-zero value of ρ. From the spectra shown in Fig. 4(e), we calculated ρ of the WS_2 PL in the WS_2/Cr_2Se_3 heterostructure at different temperatures and showed that ρ decreases from 14.3% to 2.8% as the temperature increases from 10 K to 77 K (Fig. 4(f)). The circularly polarized PL spectra of the WS_2/Cr_2Se_3 heterostructures on glassy silica and mica substrates at 10 K show similar magnetic proximity effect induced valley polarization as the heterostructures grown on SiO_2/Si (supporting information Fig. S5). This suggests that the observed temperature-dependent polarization may originate from the magnetic proximity effect by the optical control.[4,8,9] Our results demonstrated that the CVD-grown 2D Cr_2Se_3 can efficiently manipulate the spin/valley physics in ambient atmosphere, which makes them promising for practical device applications.

4. Conclusion

In summary, we have successfully synthesized thickness-tunable Cr_2Se_3 single crystal using a CVD method. We realized high-quality nonlayered Cr_2Se_3 nanosheets with thickness down to one-unit-cell (≈ 1.8 nm) and also a larger lateral length size of about 120 μm at a thicker thickness. According to crystal structure characteristics and related magnetic properties, we showed that the lattices structure of hexagonal phase Cr_2Se_3 has a–b–c sequence in space group $R\bar{3}$, with a magnetic transition temperature of approximate 75 K. Moreover, we have demonstrated the magnetic proximity effects in the WS_2/Cr_2Se_3 vdW heterostructure to manipulate the valley polarization of the adjacent WS_2. Our work paves the way for potential applications in spintronic and valleytronic devices with novel 2D magnetic materials via the magnetic proximity effect.

References

[1] Burch K S, Mandrus D and Park J G 2018 *Nature.* **563** 47

[2] Gong C, Li L, Li Z L. Ji H W, Stern A, Xia Y, Cao T, Bao W, Wang C Z, Wang Y, Qiu Z Q, Cava R J, Louie S G, Xia J and Zhang X 2017 *Nature* **546** 265

[3] Wunderlich J, Park B G, Irvine A C, Zârbo L P, Rozkotová E, Nemec P, Novák V, Sinova J and Jungwirth T 2010 *Science* **330** 1801

[4] Zhong D, Seyler K L, Linpeng X Y, Wilson N P, Taniguchi T, Watanabe K J, McGuire M A, Fu Kai-Mei C, Xiao D, Yao W and Xu X D 2020 *Nat. Nanotechnol.* **15** 187

[5] Wei P, Lee S, Lemaitre F, Pinel L, Cutaia D, Cha W, Katmis F, Zhu Y, Heiman D, Hone J, Moodera J S and Chen C T 2016 *Nat. Mater.* **15** 711

[6] Zhao C, Norden T, Zhang P Y, Zhao P Q, Cheng Y C, Sun F, Parry J P, Taheri P, Wang J Q, Yang Y H, Scrace T, Kang K F, Yang S, Miao G X, Sabirianov R, Kioseoglou G, Huang W, Petrou A and Zeng H 2017 *Nat. Nanotechnol.* **15** 187

[7] Lyons T P, Gillard D, Molina-Sánchez A, Misra A, Withers F, Keatley P S, Kozikov A, Taniguchi T, Watanabe K, Novoselov K S, Fernández-Rossier J and Tartakovskii A I 2020 *Nat. Commun.* **11** 6021

[8] Seyler K L, Zhong D, Huang B, Linpeng X Y, Wilson N P, Taniguchi T, Watanabe K, Yao W, Xiao D, McGuire M A, Fu K M C and Xu X D 2018 *Nano Lett.* **18** 3823

[9] Zhong D, Seyler K L, Linpeng X Y, Cheng R, Nikhil S, Huang B, Schmidgall E, Taniguchi T, Watanabe K, McGuire M A, Yao W, Xiao D, Fu K M C and Xu X D 2017 *Sci. Adv.* **3** e1603113

[10] Xu L X, Lu W G, Hu C, Guo Q X, Shang S, Xu X L, Yu G H, Yan Y, Wang L H and Teng J 2020 *Chin. Phys. B* **29** 077304

[11] Yin S Q, Zhao L, Song C, Huang Y, Gu Y D, Chen R Y, Zhu W X, Sun Y M, Jiang W J, Zhang X Z and Pan F 2021 *Chin. Phys. B* **30** 027505

[12] Deng Y J, Yu Y J, Song Y C, Zhang J Z, Wang N Z, Sun Z Y, Yi Y F, Wu Y Z, Wu S W. Zhu J Y, Wang J, Chen X H and Zhang Y B 2018 *Nature* **563** 94

[13] Gong C, Li L, Li Z L, Ji H W, Stern A, Xia Y, Cao T, Bao W, Wang C Z, Wang Y, Qiu Z Q, Cava R J, Louie S G, Xia J and Zhang X 2017 *Nature* **546** 265

[14] Huang B, Clark G, Klein D R, Macneill D, Navarromoratalla E, Seyler K L, Wilson N, Mcguire M A, Cobden D H, Xiao D, Jarillo-Herrero P and Xu X D 2018 *Nat. Nanotechnol.* **13** 544

[15] Liu S S, Yuan X, Zou Y C, Sheng Y, Huang C, Zhang E Z, Ling J W, Liu Y W, Wang W Y, Zhang C, Zou J, Wang K Y and Xiu F X 2017 *npj 2D Mater. Appl.* **1** 30

[16] Zhou S S, Wang R Y, Han J B, Wang D L, Li H Q, Gan L and Zhai T Y 2019 *Adv. Funct. Mater.* **29** 1805880

[17] Chu J W, Zhang Y, Wen Y, Qiao R X, Wu C C, He P, Yin L, Cheng R Q, Wang F, Wang Z X, Xiong J, Li Y R and He J 2019 *Nano Lett.* **19** 2154

[18] Cui F F, Zhao X X, Xu J J, Tang B, Shang Q Y, Shi J P, Huan Y H, Liao J H, Chen Q, Hou Y L, Zhang Q, Pennycook S J and Zhang Y F 2019 *Adv. Mater.* **32** 1905896

[19] Zhang Y, Chu J W, Yin L, Shifa T A, Cheng Z Z, Cheng R Q, Wang F, Wen Y, Zhan X Y, Wang Z X and He J 2019 *Adv. Mater.* **31** 1900056

[20] Wen Y, Liu Z H, Zhang Y, Xia C X, Zhai B X, Zhang X H, Zhai G H, Shen C, He P, Cheng R Q, Yin L, Yao Y Y, Sendeku M G, Wang Z X, Ye X B, Liu C S, Jiang C, Shan C X, Long Y W and He J 2020 *Nano Lett.* **20** 3130

[21] Huang Y, Xu K, Wang Z X, Shifa T A, Wang Q S, Wang F, Jiang C and He J 2015 *Nanoscale* **7** 17375

[22] Ahn J H, Lee M J, Heo H, Sung J H, Kim K, Hwang H, and Jo M H 2015 *Nano Lett.* **15** 3703

[23] Mutlu Z, Wu R J, Wickramaratne D, Shahrezaei S, Liu C, Temiz S, Patalano A, Ozkan M, Lake R K, Mkhoyan K. A and Ozkan C S 2016 *Small* **12** 2998

[24] Wu J, Zhang C L, Yan J M, Chen L, Guo L, Chen T W, Gao G Y, Fei L F, Zhao W Y, Chai Y and Zheng R K 2020 *J. Phys.: Condens. Matter* **32** 475801

[25] Yang P, Zou X, Zhang Z, Hong M, Shi J, Chen S, Shu J, Zhao L, Jiang S and Zhou X 2018 *Nat. Commun.* **9** 979

[26] Chen Y, Jiang Y, Yi C, Liu H W, Chen S L, Sun X X, Ma C, Li D, He C L, Luo Z Y, Jiang F, Zheng W H, Zheng B Y, Xu B Y, Xu Z Y and Pan A L 2021 *Sci. China Mater.* **64** 1449

[27] Zhang Z P, Niu J J, Yang P F, Gong Y, Ji Q Q, Shi J P, Fang Q Y, Jiang S L, Li H, Zhou X B, Gu L, Wu X S and Zhang Y F 2017 *Adv. Mater.* **29** 1702359

[28] Zhang D L, Zeng Z X S, Tong Q J, Jiang Y, Chen S L, Zheng B Y, Qu J Y, Li F, Zheng W H, Jiang F, Zhao H P, Huang L Y, Braun K, Meixner A J, Wang X and Pan A L 2020 *Adv. Mater.* **32** 1908061

[29] Zhang D L, Liu Y, He M, Zhang A, Chen S L, Tong Q J, Huang L Y, Zhou Z Y, Zheng W H, Chen M X, Braun K, Meixner A J, Wang X and Pan A L 2020 *Nat. Commun.* **11** 4442

[30] Adachi Y, Ohashi, M, Kaneko T, Yuzuri M, Yamaguchi Y, Funahashi S and Morii Y 1994 *J. Phys. Soc. Jpn.* **63** 1548

[31] Zhang Y, Yin L, Chu J W, Shifa T A, Xia J, Wang F, Wen Y, Zhan X Y, Wang Z X and He J 2018 *Adv. Mater.* **30** 1803665

[32] Zhang T T, Su X L, Yan Y G, Liu W, Hu T Z, Zhang C, Zhang Z K and Tang X F 2018 *ACS Appl. Mater. Interfaces.* **10** 22389

[33] Chen J Y, Li X X, Zhou W Z, Yang J L, Ouyang F P and Xiong X 2019 *Adv. Electron. Mater.* **6** 1900490

[34] Gong S H, Alpeggiani F, Sciacca B, Garnett E C and Kuipers L 2018 *Science* **359** 443

[35] Xiao D, Liu G B, Feng W X, Xu X D and Yao W 2012 *Phys. Rev. Lett.* **108** 196802